

# RSC Advances



This is an *Accepted Manuscript*, which has been through the Royal Society of Chemistry peer review process and has been accepted for publication.

*Accepted Manuscripts* are published online shortly after acceptance, before technical editing, formatting and proof reading. Using this free service, authors can make their results available to the community, in citable form, before we publish the edited article. This *Accepted Manuscript* will be replaced by the edited, formatted and paginated article as soon as this is available.

You can find more information about *Accepted Manuscripts* in the [Information for Authors](#).

Please note that technical editing may introduce minor changes to the text and/or graphics, which may alter content. The journal's standard [Terms & Conditions](#) and the [Ethical guidelines](#) still apply. In no event shall the Royal Society of Chemistry be held responsible for any errors or omissions in this *Accepted Manuscript* or any consequences arising from the use of any information it contains.

## ARTICLE

# Impact of Bonding at Multi-layer Graphene/Metal Interfaces on Thermal Boundary Conductance

Cite this: DOI: 10.1039/x0xx00000x

Liang Chen,<sup>a</sup> Zhen Huang,<sup>b</sup> and Satish Kumar<sup>a,†</sup>

Received ooth 0x0x xxxx,

Accepted ooth 0x0x xxxx

DOI: 10.1039/x0xx00000x

www.rsc.org/

We use density functional theory (DFT) and atomistic Green's function (AGF) to study the effect of bonding on phonon transmission and thermal boundary conductance (TBC) at the interface of metals (Cu, Au, and Ti) and single layer graphene (SLG)/multi-layer graphene (MLG). Our analysis shows that the TBC across Ti/SLG/Ti interfaces ( $\sim 500$  MW/m<sup>2</sup>K) is significantly larger than the TBC across Cu/SLG/Cu ( $\sim 10$  MW/m<sup>2</sup>K) and Au/SLG/Au ( $\sim 7$  MW/m<sup>2</sup>K) interfaces. However, the TBC across Ti/MLG/Ti ( $\sim 40$  MW/m<sup>2</sup>K) is order of magnitude lower compared to TBC at Ti/SLG/Ti interface, while TBC at Cu/MLG/Cu and Au/MLG/Au interfaces are similar to that of Cu/SLG/Cu and Au/SLG/Au, respectively. We find that this substantial decrease in TBC at Ti/MLG/Ti interface is a result of phonon mismatch between graphene layer bonded to Ti and non-bonded graphene layers. The effect of number of graphene layers on TBC at Cu/MLG/Cu and Au/MLG/Au interfaces is relatively insignificant due to the weak interactions at these metal-graphene interfaces. We observe that the moderate attenuation of Ti-C bonding strength can enhance the phonon coupling between graphene layers bonded to Ti and non-bonded graphene layers, and can increase TBC across Ti/MLG/Ti by  $\sim 100\%$ . This impact of interfacial bonding strength on TBC at metal-MLG interfaces, predicted by AGF calculations, is further confirmed by non-equilibrium molecular dynamics simulations which show the transition of thermal transport mechanism from metal/graphene dominated resistance to graphene/graphene dominated resistance as the metal/graphene bonding strength increases in metal/MLG/metal structure.

## Introduction

Extraordinary carrier mobility, thermal conductivity<sup>1</sup> and mechanical properties<sup>2</sup> of graphene have intrigued broad research interest in graphene nano-electronic devices such as field effect transistors<sup>3</sup> and optoelectronic devices.<sup>4</sup> The single layer pristine graphene sheet has very low bandgap which makes it un-suitable for logic applications.<sup>5</sup> However, bandgap of multi-layer graphene (MLG) can be tuned by controlling the stacking order while maintaining high carrier mobility.<sup>6,7</sup> The recent progress in fabrication and structure-manipulation techniques has made MLG a promising material for nano-electronic devices.<sup>8-10</sup> MLG can have considerable contact with metal electrodes in its electronic devices which can also be an important pathway of heat dissipation.<sup>11,12</sup> Many previous studies have measured thermal boundary conductance (TBC) between graphene/graphite and various metals such as Cu, Au, Ti, Al, *etc.*<sup>13-16</sup> Very low TBC has been reported for some metals such as 7-20 MW/m<sup>2</sup>K for graphene/Au interfaces.<sup>14</sup> The low TBC can hinder the effective heat removal from the nano-electronic devices leading to degradation of performance and reliability.<sup>11</sup> It is crucial to estimate TBC and decipher phonon transport mechanism at various graphene/metal

interfaces to engineer these interfaces for effective thermal management and enhanced performance.

The interfacial chemistry can significantly affect the strength of interaction as well as TBC at graphene/metal contacts.<sup>17</sup> Recent studies have shown TBC across graphene/metal interfaces depends on multiple factors such as interfacial structure,<sup>25,26</sup> bonding,<sup>18,19</sup> contaminants and defects,<sup>14,16</sup> *etc.*<sup>20,21</sup> According to different bonding type, graphene/metal interfaces can be classified into two types: physisorption interface (e.g., Au, Cu, Ag, Pt, and Al) formed by charge transfer and chemisorption interface (e.g., Ti, Co, Ni, and Pd) formed by orbital hybridization.<sup>6,22,23</sup> Several studies<sup>13-16</sup> have measured TBC at highly oriented pyrolytic graphite (HOPG) and metal interfaces. The TBC at physisorption HOPG/metal interfaces (e.g., Au, Cu, and Al) has been reported in the range of 7 to 60 MW/m<sup>2</sup>K around room temperature, while the TBC at chemisorption interfaces (e.g., HOPG/Ti) has been reported as high as 120 MW/m<sup>2</sup>K. These measurements at HOPG/metal interfaces are often used as approximations of TBC at graphene/metal interfaces. However, the impact of interfacial bonding on TBC across MLG remains unclear.

Thermal properties of MLG in electronic devices can be

very different from HOPG as i) MLG may have much smaller cross-plane dimension,<sup>24-26</sup> and ii) interaction with surrounding can significantly change phonon properties of MLG.<sup>27-30</sup> An important query, which is a topic of investigation of some recent studies,<sup>19, 25, 31-37</sup> is how the number of graphene layers ( $n$ ) in a MLG affects its thermal conductivity and TBC across its interfaces. The thickness of MLG is generally much smaller than the phonon mean free path of HOPG in cross-plane direction; therefore boundary/interface scattering of phonons is dominant for thermal transport across MLG. It has been demonstrated that the cross-plane thermal conductivity of MLG is smaller than that of HOPG and have a strong dependence on  $n$  as phonon mean free path in MLG is limited by its thickness.<sup>33, 35</sup> However, both experiments<sup>38</sup> and simulations<sup>19, 31, 32</sup> have shown that the increasing  $n$  from 3 to 10 only slightly reduces or has no effect on the TBC across embedded MLG. When  $n$  is less than or equal to three (i.e., single, bilayer or trilayer embedded graphenes), the effect of  $n$  on TBC may depend on the contact materials.<sup>19, 31, 32</sup> For SiO<sub>2</sub>/graphene interfaces, increasing graphene layers from single to few layers slightly reduces<sup>32, 38</sup> or does not changes<sup>19</sup> the TBC. The effect of  $n$  on TBC at metal/graphene interfaces becomes complicated because of the different interfacial chemistry at different metal interfaces.

Chang *et al.*<sup>31</sup> and Shen *et al.*<sup>19</sup> performed non-equilibrium molecular dynamics (NEMD) simulations to study TBC across Cu/MLG/Cu structures. Both studies have shown a larger reduction in TBC from Cu/SLG/Cu to Cu/MLG/Cu. In their MD simulations, Lennard-Jones (L-J) potential model is used to describe the Cu/graphene interactions, which have large interatomic force constants (IFCs) for Cu-C interactions.<sup>19</sup> But density functional theory (DFT) calculations have shown weak Cu/graphene interactions.<sup>21, 22, 39</sup> These different descriptions of Cu/graphene interaction can lead to very different trends and contradictory results for TBC dependence on  $n$ . The first principle study is necessary to consider the effect of bonding strength at interface and accurately decipher the effect of  $n$  on TBC across different metal/MLG/metal structures. If a graphene layer of MLG is chemically bonded to the metallic contact (e.g., graphene-Ti bonding), phonon states of this graphene layer can be significantly changed by the chemical bonds while the other graphene layers of MLG have weak interaction with the contacts and remain in pristine state.<sup>40</sup> Therefore, a large mismatch in phonon density of states between the first graphene layer (~bonded to the metal) and the adjacent graphene layers can reduce the phonon coupling between these graphene layers as well as the cross-plane thermal conductance of the MLG. Metal/graphene bonding strength has different impact on phonon coupling at metal/graphene and graphene/graphene interfaces. Strong bonding can increase phonon coupling between MLG and metal, but it creates phonon mismatch and reduce the phonon coupling among graphene layers in MLG. The interplay of these two mechanisms and the corresponding effect on thermal transport across MLG/metal interfaces remain unclear.

In order to elucidate the impact of interfacial bonding on thermal transport between MLG and different metals, we perform first principle DFT and atomistic Green's function (AGF) based calculations to investigate phonon transmission and TBC at metal/SLG/metal (Fig. 1(a)) and metal/MLG/metal (Fig. 1(b)) interfaces. We consider three different materials: Cu and Au for the weak physisorption bonding and Ti for strong chemisorption bonding. We find TBCs of Cu/SLG/Cu and Cu/MLG/Cu are comparable, which is in contrast to previous studies using molecular dynamics.<sup>19, 31</sup> We observe the similar trend for TBC at Au/MLG/Au and Au/SLG/Au interfaces. This indicates graphene/metal interface dominates the heat transfer at physisorption interfaces between MLG and metal. On the other hand for Ti/MLG/Ti structure, Ti-C interactions significantly change the phonon density of states (DOS) of graphene layer bonded to Ti and reduce its phonon coupling with adjacent graphene layer. As a result, thermal contact resistance (TCR) between these graphene layers dominates the heat transfer across Ti/MLG/Ti interfaces, and results in much smaller TBC than Ti/SLG/Ti interfaces. We investigate how the bonding strength changes the graphene/metal and graphene/graphene phonon coupling by scaling graphene/metal interatomic force constants. We demonstrate that due to the tradeoff between graphene/Ti TCR and graphene/graphene TCR, appropriate attenuation of Ti-C bonding strength across Ti/MLG/Ti interfaces can increase the TBC rather than decreasing it. The findings in this study will provide insights to understand recent experimental measurements of TBC at graphene/metal interfaces and to engineer these interfaces to enhance TBC.

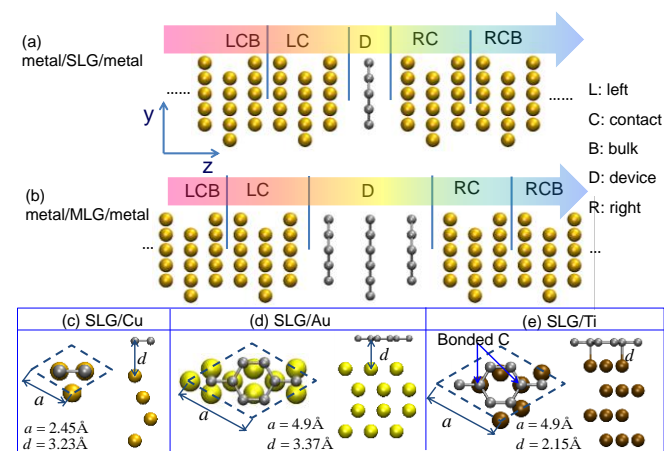


Figure 1. Schematic of (a) metal/SLG/metal system and (b) metal/MLG/metal system for the AGF calculations. Multi-layer graphene consists of single layer graphene (SLG) with AB stacking. The SLG and MLG are considered as the devices (D) which are sandwiched between two metal contacts: left contact (LC) and right contact (RC). The regions beyond LC or RC are defined as the left contact bulk (LCB) and right contact bulk (RCB), which do not interact with the device region. Views in x-y plane and x-z plane of a unit cell for (c) SLG/Cu, (d) SLG/Au and (e) SLG/Ti structures, respectively. These structures have been optimized using DFT simulations to calculate the equilibrium distance between metal and graphene. Only four layers of metal atoms are shown.

## Models and Methodology

In this study, AGF calculations are performed to determine the phonon transmission function at MLG/metal interfaces, and TBC is then calculated by Landauer formula.<sup>41-43</sup> In AGF calculations, the lattice interactions at interfaces with predefined nano-structures can be described by second order IFCs neglecting anharmonic effects. In absence of accurate empirical interatomic potential models for graphene/metal interactions, we first optimize graphene/metal structures and derive the IFCs using DFT calculations.<sup>44</sup> Figure 1 (a) and (b) show the structures of SLG/metal and MLG/metal interfaces considered in the AGF calculations. The SLG or MLG is sandwiched between two metal contacts to form the symmetrical metal/SLG/metal or metal/MLG/metal structures. The phonon transmission and TBC across the device (SLG or MLG) region involve two identical interfaces, and the values across single interface can be obtained by a multiplication of 2. A top view, in x-y plane, of the graphene/metal interfaces are shown in Fig. 1 (c), (d), and (e) for Cu, Au and Ti, respectively. Cu (111), Au (111), and Ti (0001) surfaces are cleaved to make contact with graphene sheets; these surfaces are perpendicular to z axis (see Fig. 1). In order to form periodic lattices in x and y directions, a graphene/Cu unit cell consists of one graphene unit cell while the graphene/Au and graphene/Ti unit cells consist of four graphene unit cells. Finally, we perform NEMD simulations to further validate the results of AGF calculations and examine the anharmonic effects.<sup>45</sup>

### Density Functional Theory Calculations

We use Vienna *ab initio* package (VASP) for the DFT simulations.<sup>44</sup> Plane wave basis sets with a kinetic energy cutoff of 400 eV are used in the projector augmented-wave (PAW) method.<sup>46</sup>  $32 \times 32 \times 1$  k-point grids for Cu/SLG system and  $21 \times 21 \times 1$  k-point grids for Au/SLG and Ti/SLG structures are used. The optimized in-plane lattice constant  $a$  of graphene is 2.45 Å, and the metal lattices are adjusted to match graphene lattices. With  $a=2.45$  Å, the spacings  $d$  between graphene and metal surfaces are further optimized using DFT calculations. The optimized spacing are 3.23 Å, 3.37 Å, and 2.15 Å for the Cu, Au, and Ti interfaces with graphene respectively as shown in Fig. 1 (c), (d), and (e), which is consistent with previous DFT studies<sup>22,47</sup>. The graphene/Ti spacing is quite closed to the Ti-C bonding length (2.13 Å) in a TiC crystal which indicates the chemisorption bonding for the two Ti-C pairs at graphene/Ti interface in a unit cell as shown in Fig. 1 (e). The second order IFCs for C-C, metal-metal, and metal-C atom pairs are obtained by DFT calculations using a  $5 \times 5$  supercell for Cu/SLG system and a  $3 \times 3$  supercell for Au/SLG and Ti/SLG system.<sup>48</sup> We use  $3 \times 3 \times 1$  k-point grids to sample the Brillouin zone of this supercell, and displace each atom in two directions: in plane and orthogonal to the graphene plane. The displacement magnitudes are  $\pm 0.03$  Å in both cases. Using the IFCs obtained from the DFT simulations, we construct the harmonic matrices which describe inter-atomic interactions in the AGF calculations.<sup>42</sup>

### Atomistic Green's Function Calculations

We obtain the transmission function from AGF calculations, and then use Landauer formula to calculate the TBC.<sup>43</sup>

$$\sigma = \int_0^\infty \int_{\vec{k}_\parallel} \frac{C_{ph}(\omega, T)}{2\pi} \Xi(\omega, \vec{k}_\parallel) \frac{d\vec{k}_\parallel}{(2\pi)^3} d\omega \quad (1)$$

where  $C_{ph}(\omega, T)$  is the specific heat of a phonon mode of frequency  $\omega$  at temperature  $T$ , and  $\Xi(\omega, \vec{k}_\parallel)$  is the transmission function at frequency  $\omega$  and transverse k-point  $\vec{k}_\parallel = (k_x, k_y)$ .<sup>43</sup>

$$\Xi(\omega, \vec{k}_\parallel) = \text{Trace}[\Gamma_L G_{LD, RD} \Gamma_R G_{LD, RD}^\dagger] \quad (2)$$

$\Gamma_L$  and  $\Gamma_R$  are phonon escape rate from left and right contacts while  $G_{LD, RD}$  and  $G_{LD, RD}^\dagger$  are the Green's function of device region and its complex conjugate. We construct the harmonic matrices in a finite plane-wave form so that an efficient sampling in transverse Brillouin zone  $\vec{k}_\parallel$  can be used to include the phonons of all wavelengths.<sup>41,43</sup> With the plane-wave formulation, each layer can be represented by one unit cell (Fig. 1c) and the sampling in Brillouin zone is performed with a  $\vec{k}_\parallel$  mesh of  $200 \times 200$ . The Monkhorst and Pack scheme<sup>49</sup> is used to discretize the Brillouin zone. The details about the calculation of transmission function using AGF method can be found in the References.<sup>41-43</sup>

### Non-equilibrium Molecular Dynamics Simulations

We perform the non-equilibrium molecular dynamics simulations on Cu/3LG/Cu structures using Lammmps package.<sup>50</sup> We use the optimized Tersoff potential<sup>51</sup> and embedded-atom method (EAM) potential<sup>52</sup> to describe the C-C interactions and Cu-Cu interactions, respectively. We model the interaction between C-Cu atoms at the interface using Lennard-Jones (L-J) potential:

$$V_y(r) = 4\chi\epsilon_y \left[ \left( \frac{\sigma_y}{r} \right)^{12} - \left( \frac{\sigma_y}{r} \right)^6 \right] \quad (3)$$

where  $\epsilon=25.78$  meV and  $\sigma=3.0825$  Å are taken from a study by Xu and Buehler's.<sup>53</sup> We use the parameter  $\chi$  to scale the interaction strength between C and Cu atoms,<sup>28,54</sup> which is similar to the scaling factor  $f$  in the AGF calculations. A time step of 0.5 fs is used in all simulations. The system is periodic in the cross-section perpendicular to the graphene plane. One atomic layer beyond the heating/cooling bath is fixed. The dimensions of the system are  $38.8 \text{ Å} \times 42.3 \text{ Å} \times 267.5 \text{ Å}$  and the total number of atoms in system is 40,392. Each system is first equilibrated in NVT at 300K for 0.5 ns and in NVE for another 0.5 ns. Then a heat rate of  $\pm 45$  nW is applied at the heating/cooling bath which consists of 3519 atoms. Each case is simulated for 5 ns to first obtain a steady state, and then the data is sampled for additional 5 ns which is used for the estimation of temperature profiles.

## Results and Discussions

### SLG and Metal Substrates Interactions

The bonding between graphene and metal atoms at the interface can be illustrated by the distribution of electron localization function (ELF) as shown in Fig. 2. ELF describes chemical bonds by the probability of finding another same-spin electron in the neighborhood of a reference electron.<sup>55</sup> ELF is normalized to have values between 0 and 1, where ELF=1 corresponds to complete localization and ELF=0.5 corresponds to uniform electron gas.<sup>56</sup>

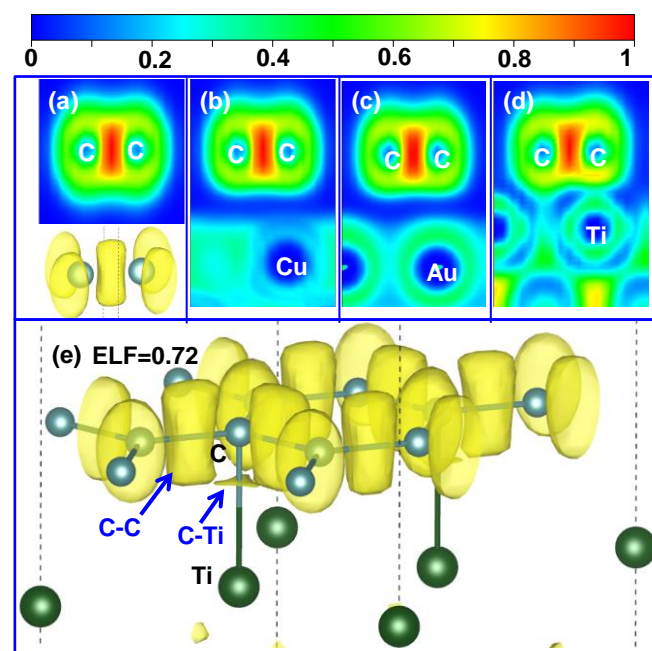


Figure 2. Electron localization function (ELF) for isolated single layer graphene (SLG) and SLG on metal substrates. (a) ELF contour and iso-surfaces with ELF=0.72 for isolated SLG; (b) ELF contour for SLG on Cu (111); (c) ELF contour for SLG on Au (111); (d) ELF contour for SLG on Ti (0001); (e) ELF iso-surfaces with ELF=0.72 for SLG on Ti (0001). The arrows in (e) indicates the electron localization between C atoms in SLG and between C and Ti atoms at SLG/Ti interface, respectively.

Figure 2 (a) shows the ELF contour of a unit cell of SLG in a cross-section perpendicular to SLG sheet and containing a C-C bond.<sup>57</sup> The red region with high ELF values between two C atoms indicates C-C  $sp^2$  bonding in SLG while the lower part of Fig. 2 (a) shows the iso-surfaces of ELF=0.72. Figure 2 (b) to (d) show the ELF contour around C and metal atoms at SLG-metal interfaces. At SLG-Cu or SLG-Au interface, electron localization is not observed and the ELF distribution of SLG remains almost same as isolated SLG. However, the strong interaction with Ti has distorted the ELF distribution of SLG. The overlap in ELF of SLG and Ti can be observed in Fig. 2 (d). Figure 2 (e) shows the iso-surfaces of ELF=0.72 at SLG-Ti interface. A strong electron localization can be observed at SLG-Ti interface between C and Ti atoms, whose position is closer to C atom. This indicates that the two C atoms located just above Ti atoms in a unit cell (see Fig. 1 (e)) make chemical bonds with corresponding Ti atoms, while other six C atoms of

the unit cell are not bonded to Ti. Gengler *et al.* examined the interfacial chemistry for thin titanium films deposited on HOPG using X-ray photoelectron spectroscopy, and showed that Ti-C can be formed at Ti/HOPG interface depending on the deposition conditions which is consistent with our simulations.<sup>16</sup> The ELF for non-bonded C atoms is also distorted (see Fig. 2 (d)) but electron localization is not observed.

In order to investigate the effects of graphene-metal interaction on phonon distribution, we calculate the phonon density of states (DOSs) of the SLG supported on metal substrate using IFCs estimated from the DFT simulations. Figures 3 (a) shows the DOSs of isolated SLG while Fig. 3 (b) to (d) show the DOSs of SLG supported on Cu (111), Au (111), and Ti (0001), respectively. Comparing to the DOSs of isolated SLG, the major changes in DOSs of SLG supported on Cu (111) and Au (111) are around zero frequency and high frequency region, which are associated with the effects of Cu (111) or Au (111) substrate on acoustic and optical phonon modes near the zone-center ( $\Gamma$  point), respectively. As shown in Fig. 3 (b) and (c), the DOSs near zero-frequency is first suppressed and then increased rapidly with a small overshoot near 1.2 THz and 1.7 THz for SLG/Cu and SLG/Au structures, respectively. This is due to the interactions with substrate which break the symmetry of SLG for out-of-plane acoustic (ZA) modes and ZA modes near zone-center leading to non-zero frequencies for these modes at zone center.<sup>21, 27</sup> A high frequency peak ( $\sim 49$  THz) in SLG DOSs is indicated by a solid arrow in Fig. 3 (a) which can be attributed to the longitudinal and transverse optical modes near zone-center. The physisorption interactions with substrate soften the LO and TO modes near zone-center to lower frequencies and create the peaks around 46.4 THz and 47.2 THz which are indicated by hollow arrows in Fig. 3 (b) and (c).<sup>21, 27</sup>

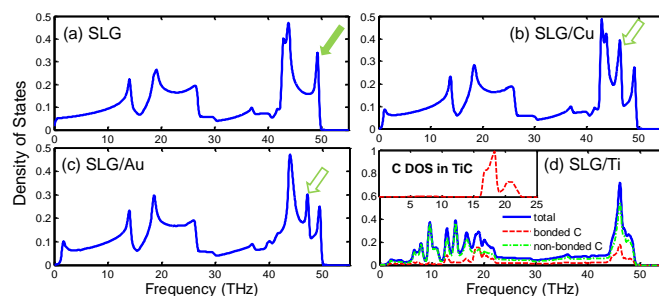


Figure 3. Phonon density of states (DOSs) of (a) isolated single layer graphene (SLG), (b) SLG on Cu (111), (c) SLG on Au (111) and (d) SLG on Ti (0001). The DOSs in (d) is decomposed to partial DOSs of Ti-bonded C atoms and non-bonded C atoms. The inset in (d) shows the partial DOSs of C atoms in TiC crystal. The scale of y-axis in inset is from 0 to 1. The partial DOSs of C in TiC diminish to zero beyond 25 THz. The solid arrow in (a) indicates the optical phonon states near zone-center in isolated SLG while hollow arrows in (b) and (c) indicate the phonon states due to softening of optical phonon states near zone-center by Cu or Au substrate.

In contrast to physisorption interactions, the chemisorption interactions with Ti substrate substantially change the DOSs of SLG as shown in Fig. 3 (d). As discussed during the analysis of

ELF for SLG/Ti system, two C atoms located just above the Ti atoms are bonded with Ti atoms while the other six C atoms are not bonded. The DOSs of SLG is decomposed to the partial DOSs of these two types of C atoms as shown in Fig. 3 (d). The partial DOSs of both bonded and non-bonded C atoms are significantly changed throughout the phonon spectrum due to the strong SLG-Ti interactions. SLG-Ti (0001) spacing  $d$  ( $\sim 2.17$  Å) is close to Ti-C bond length ( $\sim 2.13$  Å)<sup>58</sup> in TiC. In addition, the peak in phonon DOSs around 20 THz also agrees with the DOSs of C atoms in TiC as shown in the inset of Fig. 3 (d), which implies chemical interactions between Ti and C atoms in SLG/Ti (0001) system is similar to TiC.

### Phonon Transmission and TBC across metal/SLG/metal Interfaces

Figure 4 shows the phonon transmission functions across metal/SLG/metal interfaces calculated from the AGF method. The sizes of a unit cell in three metal/graphene systems are different (see Fig. 1). For comparison, we divide the transmission functions by the number of SLG primitive unit cells (with two C atoms) in the corresponding metal/graphene system. Because of the harmonic assumption in the AGF method, only phonons of same frequency can interact at the interfaces. Since the phonon spectrum of Cu, Au and Ti are below 10 THz and much smaller than the phonon spectrum of SLG (up to 50 THz), the phonon transmission is also restricted to frequencies below 10 THz. The coupling between higher-frequency phonons in SLG and phonons in metal contacts is neglected in AGF calculations. However, its contribution to the phonon transport is not significant unless high pressure is applied to enhance the SLG/substrate interactions.<sup>20</sup>

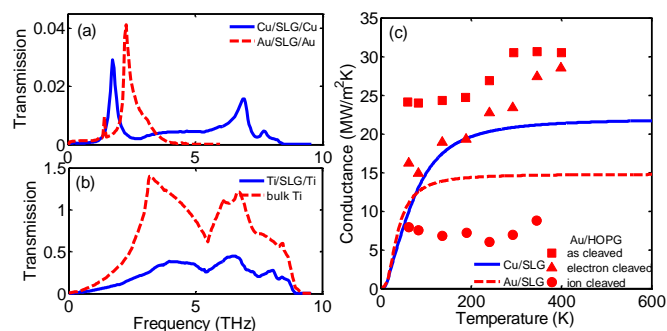


Figure 4. Phonon transmission as a function of frequency in (a) Cu/SLG/Cu and Au/SLG/Au structures and (b) Ti/SLG/Ti system and bulk Ti. (c) Thermal boundary conductance (TBC) at Cu/SLG and Au/SLG interfaces as a function of temperature (lines from current work). Experimental measurement (markers)<sup>14</sup> of TBC at Au/HOPG interfaces for three different methods of surface treatment (as cleaved, electron cleaved and ion cleaved) of HOPG before Au deposition.

As shown in Fig. 4 (a), the transmission functions across Cu/SLG/Cu and Au/SLG/Au interfaces are very small ( $< 0.04$ ). The frequency of the first peak in the transmission curve of Cu/SLG/Cu or Au/SLG/Au system corresponds to the peak in DOSs of sandwiched SLG (see Fig. 3 (b) and (c) near zero-frequency). The transmission function across Ti/SLG/Ti interfaces (see Fig. 4 (b)) is much larger than Cu/SLG/Cu and

Au/SLG/Au structures because of the strong bonding strength at SLG/Ti interfaces with chemisorption interactions. Also shown in Fig. 4 (b) is the transmission function in bulk Ti crystal with pristine lattices. Ti/SLG interface have reduced phonon transmission in comparison to the Ti/Ti interface, but the transmission function across Ti/SLG/Ti resembles with bulk Ti and has similar order of magnitude, which indicates good phonon coupling at Ti/SLG interface.

The TBCs in the three systems are calculated by Landauer formula using the transmission function estimated from the AGF calculations. Figure 4 (c) shows TBC as a function of temperature at Cu/SLG and Au/SLG interfaces calculated from the AGF calculations and compare against the experimental measurements at Au/HOPG interfaces from Ref.<sup>14</sup>. In absence of inelastic scattering at metal/SLG interfaces, TBC estimated from AGF calculations saturates to 21.5 MW/m<sup>2</sup>K and 14.4 MW/m<sup>2</sup>K around  $\sim 400$  K and  $\sim 200$  K for Cu/SLG and Au/SLG interfaces, respectively. These temperatures are close to their Debye temperature (343.5 K for Cu and 170 K for Au) above which all phonon modes are excited. The surface treatment of HOPG can lead to different surface impurity, defects and roughness and thereby significantly change the TBC as shown in Fig. 4(d) for three different surface treatments (as cleaved, electron cleaved and ion cleaved HOPG) before Au deposition. Our AGF calculations consider smooth Au/SLG interface without any defects or contaminants. The prediction of TBC at Au/metal interface by AGF lies between the highest and lowest values of experimental measurements at Au/HOPG interfaces considering three different surface treatments. Considering the difference in the interface conditions, the agreement between our AGF predictions and experiment measurements is reasonably good. However, the AGF calculations predict extremely large TBC ( $\sim 1000$  MW/m<sup>2</sup>K around room temperature) for Ti/SLG/Ti system, which is about one order of magnitude larger (see Fig. 6) than the experimental measurements at Ti/HOPG interface ( $\sim 120$  MW/m<sup>2</sup>K around room temperature).<sup>5, 38</sup> Besides the different interface condition between Ti/SLG interfaces in AGF calculations and Ti/HOPG interfaces in experiments, the difference in the phonon transport mechanism at Ti/SLG and Ti/MLG interfaces may also play an important role which has not been explored before and will be discussed in the next section.

### Phonon Transmission and TBC across metal/MLG/metal Interfaces

For the phonon transport analysis at metal/MLG interfaces, two contact resistances should be considered: (1)  $R_{MG}$  which is associated with the coupling of phonons between metal and first layer of MLG; this is investigated in previous section using metal/SLG/metal structures, and (2)  $R_{GG}$  which is related with the phonon coupling between first layer of graphene with the following graphene layer due to different phonon DOSs (see Fig. 5b). In the metal/MLG/metal system, metal contacts have either physisorption or chemisorption interactions with the first layer of MLG which can significantly change phonon DOSs of this graphene layer (see Fig. 3). Therefore, significant

mismatch in phonon DOSs may exist between the first layer of MLG and following layer which results in the thermal contact resistance  $R_{\text{CG}}$  in the AGF calculations. This phonon mismatch between layers of graphene depends on the interaction strength with metal contact: physisorption interaction results in small phonon mismatch (Fig. 3 (b) for Cu/SLG and (c) for Au/SLG) while chemisorption interaction leads to a significant phonon mismatch (Fig. 3 (d) for Ti/SLG). In order to quantify the effects of metal/graphene interaction on the phonon coupling at two types of interfaces, we perform AGF calculations for metal/MLG/metal structures (Fig. 1 (b)) for different number of graphene layers ( $1 \leq n \leq 31$ ) and study the phonon transmission and TBC at metal/MLG interfaces.

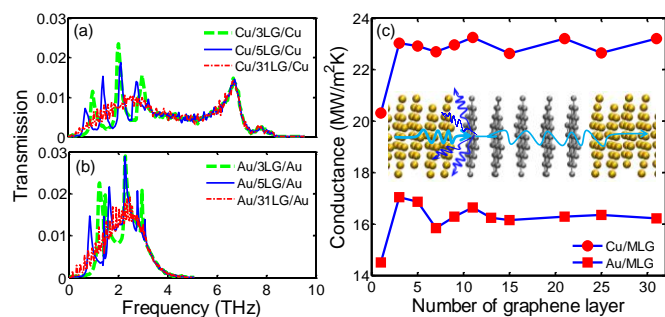


Figure 5. Phonon transmission as a function of frequency in (a) Cu/MLG/Cu structures and (b) Au/MLG/Au structures. (c) TBC at Cu/MLG and Au/MLG interfaces as a function of number of graphene layers. The inset chart in (c) shows the dominant phonon scattering is at metal/graphene interface.

Figure 5 (a) and (b) show the phonon transmission function across Cu/MLG/Cu and Au/MLG/Au interfaces for different  $n$ . The transmission function across metal/MLG are characterized with multi-peaks at frequencies below 4 THz; the number of peaks equals the number of graphene layers, e.g., 3 or 5 peaks for  $n=3$  or  $n=5$  in Fig. 5 (a) and (b). As the number of graphene layers increases, the peaks diminish and become indistinguishable, e.g., transmission across 31 layers of graphene as shown in Fig. 5 (a) and (b). Beyond 4 THz, the transmission curves change insignificantly with increasing  $n$ . The transmission function from our AGF calculations is consistent with the transmission coefficients obtained from the wave-packet simulations using MD by Shen, *et al.*<sup>19</sup> The study in Ref.<sup>19</sup> only considered the transmission of longitudinal acoustic (LA) phonons; a fine sampling in longitudinal wave vectors and incidence angles requires a huge number of simulations as wave-packets need to be generated for each case. Our AGF calculations use plane-wave formulation with a fine sampling in transverse Brillouin zone  $\vec{k}_{\parallel} = (k_x, k_y)$ . Therefore we can efficiently incorporate the transmission of all phonon modes from different incidence angles.

The peaks and valleys in transmission curves (Fig. 5) can be explained by the phonon interference effects.<sup>19</sup> The addition of graphene layers between metal contacts increase the thickness of MLG as well as the wavelength range of allowed phonon waves so that a new peak in transmission function is created with the addition of a new graphene layer. According to Ref.

<sup>19</sup>, the oscillatory period in frequency  $\Delta f$  depends on the group velocity  $v$  of transmitting phonons and thickness of MLG  $t$ :  $t = v/2\Delta f$ . The averaged group velocity of LA phonons in bulk graphite is around 1989 m/s where the group velocities at each wave vector is calculated by  $v(q) = d\omega/dq$ . We extract  $\Delta f$  from Fig. 5 (a) and (b) and calculate  $v/2\Delta f$ . A good agreement is observed between  $v/2\Delta f$  and the corresponding MLG thickness  $t$  for both Cu/MLG/Cu and Au/MLG/Au structures, which indicates that the transmitting phonons may be dominated by LA phonons. This is also consistent with Ref.<sup>19</sup> where only transmission of LA modes was calculated. Alternatively, we can interpret the peaks and valleys of transmission function in terms of phonon coupling. Increasing number of graphene layers introduce inter-layer phonon modes in MLG and opens new channels for phonon coupling with phonons in metal contact. The peaks in transmission function represent good coupling between phonons in metal contacts and inter-layer phonon modes of MLG. The peaks of transmission curve are below 4 THz because the phonon modes of MLG in cross-plane direction have a spectrum below 4 THz.<sup>25, 59</sup>

In comparison to the transmission function across Cu/SLG/Cu and Au/SLG/Au (Fig. 4 (a)), the magnitude of transmission function across Cu/MLG/Cu and Au/MLG/Au interfaces does not change significantly. This indicates that the small phonon mismatch between first layer of graphene and the following layers does not introduce a large  $R_{\text{CG}}$ . Figure 5 (c) shows the TBC at Cu/MLG and Au/MLG interfaces as a function of  $n$ . The TBC increases by 2 to 3 MW/m<sup>2</sup>K for Cu (~20 to 23 MW/m<sup>2</sup>K) or Au contacts (~14 to 17 MW/m<sup>2</sup>K) when  $n$  increases from one to two. Further increasing graphene layers have little effect on TBC for both Cu/MLG and Au/MLG interfaces which is also observed in MD simulations for Cu/MLG/Cu structure in previous studies.<sup>19, 31</sup> This trend seems counterintuitive because adding graphene layers will increase  $R_{\text{CG}}$  and reduce the overall thermal conductance. Phonon mismatch between the first graphene layer and the following graphene layer caused by the weak physisorption interaction with Cu or Au is small resulting in small  $R_{\text{CG}}$ . So,  $R_{\text{MG}}$  dominates the thermal transport while  $R_{\text{CG}}$  can be negligible for Cu/MLG or Au/MLG interfaces as illustrated in the inset of Fig. 5(c). Recent MD simulations<sup>19, 31</sup> predicted different trend for TBC across Cu/MLG/Cu, i.e., TBC decreases significantly from Cu/SLG/Cu to Cu/MLG/Cu. It should be noted that the L-J potential is used in these studies and corresponding IFCs are much larger than IFCs predicted by our DFT simulations, which will be discussed in the foregoing section on NEMD simulations. IFCs are indications of bonding strength between Cu and graphene. The metal/graphene bonding strength does not only affect the phonon coupling at metal/graphene interfaces but also the phonon coupling among graphene layers; its impact on phonon transmission and TBC can be different for metal/SLG/metal and metal/MLG/metal structures, which will be demonstrated next for Ti/MLG/Ti structure.

In comparison to Cu/MLG or Au/MLG interfaces, Ti/MLG interface has negligible  $R_{\text{MG}}$  which is reflected in high TBC at Ti/SLG interface (~1000 W/m<sup>2</sup>K). As  $R_{\text{MG}}$  is low, phonon

coupling between graphene layers with distinct phonon DOSs and the associated  $R_{\text{GG}}$  may become important for the thermal transport at Ti/MLG interfaces. Figure 6 (a) shows the phonon transmission function across Ti/MLG/Ti structure with  $n$  from 1 to 25. The transmission across Ti/MLG/Ti structure with three graphene layers ( $n=3$ ) is one order of magnitude smaller than the Ti/SLG/Ti ( $n=1$ ) structure (Fig. 4 (b)). As  $n$  increases beyond three, the magnitude of transmission function changes slightly. This suggests good phonon coupling among middle graphene layers and weak phonon coupling at the interface between the first graphene layer and the following layer as expected from the significant mismatch of phonon DOSs (Fig. 3 (a) and (d)). Similar to Cu/MLG/Cu and Au/MLG/Au structures, the transmission curves of Ti/MLG/Ti structures also have multiple peaks below 4 THz. But the number of peaks is less than the number of graphene layers by two, which is equal to the number of graphene layers not bonded with Ti contacts. The peaks in transmission curves are associated with the interference between propagating and reflected phonons. The interference effects are only observed for the middle graphene layers in Ti/MLG/Ti structures, which can be explained by the coupling mechanism between phonons in metal contacts and inter-layer phonon modes of MLG. Due to the significant mismatch in phonon DOSs with the middle graphene layers, the two graphene layers bonded to Ti contacts do not contribute in the formation of the inter-layer phonon modes<sup>36, 37</sup> as in the case of Cu/MLG/Cu or Au/MLG/Au structures, and their coupling with Ti contacts does not reflect as peak in transmission curves.

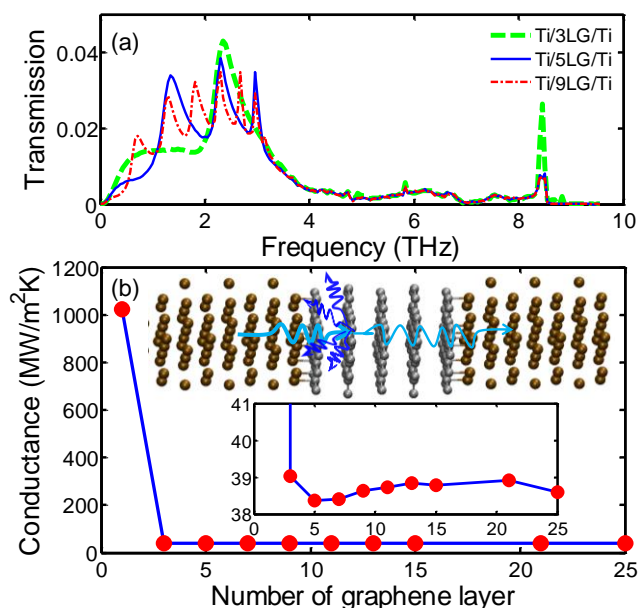


Figure 6. (a) Phonon transmission as a function of frequency in Ti/MLG/Ti structures. (b) TBC at Ti/MLG interfaces as a function of number of graphene layers. The upper inset in (b) shows the dominant phonon scattering is at the interface between graphene bonded to Ti and the following graphene layer. The lower inset in (b) shows TBC variations for  $n \geq 3$ .

The significant reduction in transmission function and TBC in Ti/MLG/Ti structure by increasing  $n$  from one to three implies the importance of phonon scattering at interfaces between graphene layers due to significant phonon mismatch. Due to the harmonic assumption in AGF calculations, the phonon scattering is not realized among the non-bonded graphene layers of nearly identical phonon DOSs. So, the change in TBC is very small in the Ti/MLG/Ti system as  $n$  increases beyond three. The AGF calculations predict TBC of 39 W/m<sup>2</sup>K at 300K for smooth Ti/HOPG interfaces, which is in agreement with the experimental measurements of TBC at Ti/HOPG interfaces ( $\sim 70 - 100$  W/m<sup>2</sup>K around room temperature).<sup>15, 16, 38</sup> Most of the experimental measurements have been performed for Ti/HOPG structures or Ti/MLG/SiO<sub>2</sub> structures and so the dramatic decrease of TBC by increasing  $n$  from one to three has never been reported for metal/MLG/metal structures. It will be worthwhile to examine these using advanced measurement techniques such as time domain thermal reflectance. Besides, the Ti/graphene interfaces in experiments may not be as smooth and clean as considered in the AGF calculations; the defects and roughness can change the Ti/graphene bonding strength and also number the number of bonded atoms at the interface. The decrease in Ti/graphene bonding strength will increase  $R_{\text{MG}}$ , but the decrease of Ti/graphene bonding strength can attenuate the mismatch in phonon properties of the first and second graphene layers leading to a decrease in  $R_{\text{GG}}$ . So, the change in TBC across Ti/MLG/Ti will depend on the interplay between  $R_{\text{MG}}$  and  $R_{\text{GG}}$ . To better understand this interplay, it is important to examine how the TBC will change if the bonding strength between Ti/graphene is scaled down.

### Manipulating TBC across metal/MLG/metal Interfaces by Tuning Bonding Strength

We have demonstrated that the interfacial bonding strength have different effects on  $R_{\text{GG}}$  and there is a tradeoff between  $R_{\text{MG}}$  and  $R_{\text{GG}}$  which suggests a method to manipulate TBC across metal/MLG/metal interfaces by tuning bonding strength. We performed a series of AGF calculations on both metal/SLG/metal and metal/MLG/metal structures by scaling the force constants (using a factor  $f$ ) for SLG-metal interactions obtained from the DFT simulations. X-ray photoelectron spectroscopy of thin titanium films deposited on HOPG shows characteristics of partial carbide bonds at the Ti/HOPG interface which depends on the deposition conditions.<sup>16</sup> Changing deposition conditions (e.g., changing energy of sputtering) can be analogous to changing  $f$  in the present study.

Figure 7 (a) and (b) show the TBC (normalized with TBC  $G_0$  at  $f=1$ ) at 300 K as a function of scaling factor  $f$  for Ti/SLG/Ti, Ti/3LG/Ti, Cu/SLG/Cu and Cu/3LG/Cu structures. Since the bonding strength at chemisorption interface between Ti and graphene is inherently strong, we can scale it down in order to reduce  $R_{\text{GG}}$ , but increase  $R_{\text{MG}}$ . On the contrary, the physisorption interaction at Cu/graphene or Au/graphene interfaces is weak, so we need to enhance the bonding strength

in order to reduce  $R_{MG}$ , but increase  $R_{GG}$ . As shown in Fig. 7 (a), the normalized TBC  $G/G_0$  across Ti/3LG/Ti interfaces increases with decreasing  $f$ , achieves peak value at  $f=0.1$  and then rapidly decreases to zero. But, the  $G/G_0$  across Ti/SLG/Ti interfaces decreases monotonically to zero with the decreasing  $f$  because  $R_{GG}$  is absent and  $R_{MG}$  increases with the decreasing  $f$ . At  $f=0.1$ , the TBC across Ti/3LG/Ti at 300 K is increased by 100% and reaches 80 W/m<sup>2</sup>K. Similar to the Ti interfaces, a peak is observed in  $G/G_0$  for Cu/MLG/Cu but not for Cu/SLG/Cu system as we increase  $f$  from 1 to 8, as shown in Fig. 7 (b). Previous non-equilibrium MD studies have shown TBC across Cu/SLG/Cu can be much larger than TBC across Cu/MLG/Cu but TBC for SiO<sub>2</sub>/SLG and SiO<sub>2</sub>/MLG interfaces are not very different. Our AGF calculations for the metal/MLG/metal structures with three different metals indicate the metal/graphene bonding strength and phonon coupling among MLG are responsible for the different trends with increasing  $n$  for different substrates.

Figure 7 (c) shows the variations of normalized TBC  $G/G_0$  across Cu/MLG/Cu structure with increasing  $n$  for different scaling factors  $f$  (~1-4). For  $f$  equal to one, the TBC increases when  $n$  is increased from one to two, but this trend in TBC variation with  $n$  is reversed when  $f$  is increased to two. Further increasing  $f$  (to 3 or 4) lead to even sharper decrease in TBC when  $n$  is increased from one to two. TBC is almost constant when  $n>3$  for all values of  $f$  considered here. Comparison of the reduction in TBC across Cu/MLG/Cu against previous MD simulation results<sup>19, 31</sup> suggests that L-J potential corresponds to these high values of  $f$ . That is why previous MD simulations<sup>19, 31</sup> predict different trend of TBC for Cu/MLG/Cu structures with increasing  $n$  than our DFT and AGF calculations ( $f=1$ ). This also suggests that first principle simulations are important to accurately present the interfacial interactions.

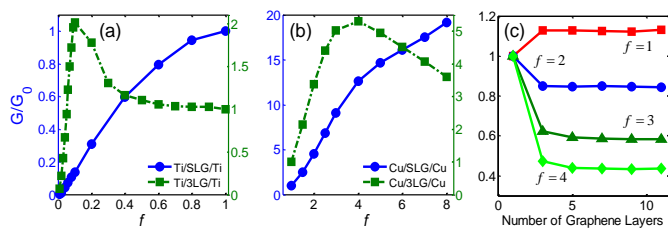


Figure 7. Normalized thermal boundary conductance (TBC)  $G/G_0$  as a function of scaling factor  $f$  in (a) Ti/SLG/Ti and Ti/3LG/Ti structures, (b) Cu/SLG/Cu and Cu/3LG/Cu structures.  $G_0$  is the TBC in the system with  $f=1$ . (c)  $G/G_0$  as a function of number of graphene layers  $n$  at different  $f$  for Cu/MLG/Cu structure.  $G_0$  is the TBC in the system with  $n=1$ .

### NEMD Simulations of Cu/MLG/Cu Structures with Different Interaction Strength

The thermal resistance between non-bonded graphene layers of MLG with similar DOSs is neglected in our AGF calculations due to the harmonic approximations. In order to justify the findings of AGF calculations for metal/MLG/metal interfaces, we perform NEMD simulations for Cu/SLG/Cu and Cu/3LG/Cu structures as MD naturally includes all anharmonic interactions (Fig. 8 (a) and (b)). The interactions between Cu

and graphene are described using L-J potential, and the scaling factor  $\chi$  is used to strengthen the interactions which are similar to scaling up  $f$  in the AGF calculations. Figure 8 (c) to (h) show the temperature profiles from the heating bath to cooling bath under a constant heating/cooling rate of  $\pm 45$  nW in Cu/SLG/Cu and Cu/3LG/Cu structures with  $\chi=1.0$ ,  $\chi=0.2$ , and  $\chi=4.0$ . Table 1 summarizes the corresponding results at steady state including the equilibrium spacing between Cu and graphene  $d_{MG}$ , the equilibrium spacing between graphene layers  $d_{GG}$ , the temperature difference between Cu and graphene  $\Delta T_{MG}$ , the temperature difference across graphene layers  $\Delta T_{MLG}$ , and TBC  $G$  across the interfaces.

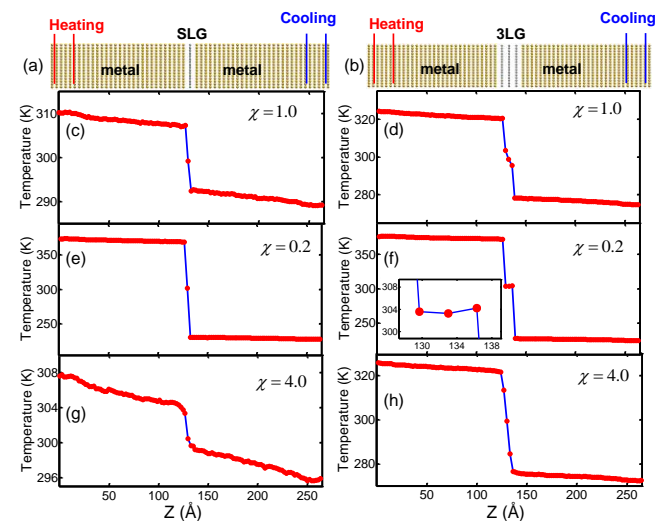


Figure 8. Schematic of (a) Cu/SLG/Cu and (b) Cu/3LG/Cu structures for non-equilibrium molecular dynamics simulations. Temperature profiles across Cu/SLG/Cu for (c)  $\chi=1.0$ , (e)  $\chi=0.2$ , and (g)  $\chi=4.0$ . Temperature profiles across Cu/3LG/Cu for (d)  $\chi=1.0$ , (f)  $\chi=0.2$ , and (h)  $\chi=4.0$ .  $\chi$  is the scaling factor in Lennard-Jones potential model for Cu/graphene interactions. The inset in (f) shows the close up of temperature profile in three graphene layers.

As shown in Table 1, the change of  $d_{MG}$  ( $\sim 0.01$  Å) is negligible as  $\chi$  increases from 1 to 3 when  $\chi=1$ . The same interfacial structure indicates same interaction strength between Cu and graphene in the two structures. However, under the same heat flux,  $\Delta T_{MG}$  increases from 7.3 K to 17.1 K, and  $\Delta T_{MLG}$  is non-negligible (8.1 K) in Cu/3LG/Cu. As a result,  $G$  decreases from 183.5 to 64.9 MW/m<sup>2</sup>K as shown in Table 1. The decrease ( $\sim 65\%$ ) in  $G$  with increasing  $n$ , when  $\chi=1$ , is also observed in the NEMD studies by Chang *et al.*<sup>31</sup> and Shen *et al.*<sup>19</sup> Here we clearly show, by comparing  $\Delta T_{MG}$  and  $\Delta T_{MLG}$  between Cu/SLG/Cu and Cu/3LG/Cu structures, adding graphene layers into Cu/SLG/Cu structures leads to the increase of both  $R_{MG}$  and  $R_{GG}$ . As the interaction strength between Cu and graphene is same in Cu/SLG/Cu and Cu/3LG/Cu structures, we can reasonably infer that the addition of graphene/graphene interfaces reduces phonon transmission in Cu/3LG/Cu structures when  $\chi=1$ .

TABLE 1. NEMD simulation results for heat transfer under constant heat flux across Cu/SLG/Cu and Cu/MLG/Cu structures with different scaling factor  $\chi$  in Lennard-Jones potential model: equilibrium spacing between Cu and graphene  $d_{\text{MG}}$ , the equilibrium spacing between graphene layers  $d_{\text{GG}}$ , the temperature difference between Cu and graphene  $\Delta T_{\text{MG}}$ , the temperature difference across graphene layers  $\Delta T_{\text{MLG}}$ , and TBC  $G$  across the interfaces.

	$\chi=1.0$		$\chi=0.2$		$\chi=4.0$	
	$n$					
$d_{\text{MG}}$ (Å)	1	3	1	3	1	3
$d_{\text{GG}}$ (Å)	N/A	3.29	N/A	3.31	N/A	3.18
$\Delta T_{\text{MG}}$ (K)	7.3	17.1	68.8	72.2	2.0	8.1
$\Delta T_{\text{MLG}}$ (K)	Neg.	8.1	Neg.	Neg.	Neg.	28.8
$G$ (MW/m <sup>2</sup> K)	183.5	64.9	19.9	19.0	693.4	60.7

It is worth noting that TBC predicted by NEMD simulations with L-J potential ( $\chi=1$ ) is much larger than TBC predicted by AGF calculations using IFCs from the DFT simulations. It implies the interaction strength described by L-J potential is much stronger than that predicted by DFT calculations. Due to the strong Cu/graphene interaction specified by the L-J potential in MD simulations, significant phonon mismatch is created between graphene layer in contact with Cu and the middle graphene layer in the Cu/3LG/Cu structure. Based on the analysis of DOSs using AGF calculations in the previous sections, it can be inferred that the interfacial phonon coupling is weak at graphene/graphene interfaces due to large phonon mismatch. Therefore, in the NEMD simulations, the hot phonons emitted from heating bath will be reflected back to the left Cu contact by graphene/graphene interfaces, which reduces the phonon transmission as well as TBC across Cu/3LG/Cu structure and increases both  $\Delta T_{\text{MG}}$  and  $\Delta T_{\text{MLG}}$ .

For a better comparison between the predictions of NEMD and AGF calculations, we need to use similar interaction strength at Cu/graphene interfaces. So we reduce  $\chi$  to 0.2 in L-J potential model, and perform NEMD simulations under the same heat flux. As shown in Table 1, TBC predicted by NEMD simulations at  $\chi=0.2$  is significantly reduced to 19.9 and 19.0 MW/m<sup>2</sup>K for Cu/SLG/Cu and Cu/3LG/Cu structures, respectively, which is comparable to the predictions by AGF calculations. For Cu/3LG/Cu structure,  $\Delta T_{\text{MLG}}$  is not distinguishable while the temperature difference across Cu/graphene interfaces  $\Delta T_{\text{MG}}$  is noticeable. So TBC only decreases by ~5% as  $n$  increase from 1 to 3, which is similar to that of SiO<sub>2</sub>/MLG/SiO<sub>2</sub> structures in the NEMD simulations by Shen *et al.*<sup>19</sup> This also confirms our AGF calculations: the phonon transport is ballistic through MLG in the metal/MLG/metal structure with weak metal/graphene interaction strength.

Similarly, by scaling  $\chi$  to 4 in the NEMD simulations, we study the phonon transport across metal/MLG/metal structures with strong interaction strength. As shown in Fig. 8 (g), the temperature variation in Cu/SLG/Cu structure becomes nonlinear near the Cu/graphene interface because the strong interfacial interaction increases phonon scattering and reduces the thermal conductivity of the near-interface region of the

semi-infinite Cu contact.<sup>60</sup> With the same interfacial interaction strength ( $\chi=4$ ), the temperature variation remains linear in the Cu/3LG/Cu structure. This implies the effects of interfacial atomic reconstruction of the metal contact are more important in metal/SLG/metal structure with strong interaction strength. As shown in Table 1,  $\Delta T_{\text{MLG}}$  has been larger than  $\Delta T_{\text{MG}}$  in Cu/3LG/Cu at  $\chi=4$ , which suggests thermal resistance at graphene/graphene interface becomes more important for metal/MLG/metal structures with strong interaction strength. As a result, TBC decreases by one order of magnitude as  $n$  increases from 1 to 3, which is similar to the Ti/SLG/Ti and Ti/MLG/Ti structures in the AGF calculations.

Finally, by NEMD simulations, we demonstrate the increase of  $\Delta T_{\text{GG}}$  with  $\chi$  because the increasing Cu/graphene interaction strength leads to larger mismatch in phonon DOSs and reduced phonon coupling between the first and middle graphene layer, which is consistent with results of AGF calculations. This also confirms that trends in TBC with increasing  $n$  for different metal/MLG/metal structures considered in this study will be valid even after including anharmonic interactions in the AGF calculations.

## Conclusions

In conclusion, we have investigated the impact of interface bonding on the phonon transmission and TBC at metal/SLG and metal/MLG interfaces. We observe strong electron localization at Ti/graphene interface as a result of the chemisorption interactions; these strong interactions significantly change the phonon DOSs of graphene layer in immediate contact with metal. The physisorption interactions of graphene with Cu and Au only change the graphene DOSs around the Brillouin zone-center. Due to this difference in interfacial interactions, the dominant thermal resistance in Cu/MLG/Cu and Au/MLG/Au structures is at the interface of metal and first layer of graphene while the thermal resistance at the interface between the first graphene layer bonded to Ti and middle graphene layers is more important in Ti/MLG/Ti structures. We have shown that the TBC can be enhanced through a moderate attenuation of bonding strength at Ti/MLG interfaces which will reduce the mismatch in phonon DOSs between graphene layers and effectively enhance the phonon

coupling between Ti and MLG. In order to validate our AGF calculations and check the effects of anharmonic interactions, we perform NEMD simulations for Cu/SLG/Cu and Cu/MLG/Cu structures. By increasing Cu/graphene interaction strength in Cu/MLG/Cu structure, we show the thermal resistance at graphene/graphene interface becomes important and exceeds the thermal resistance at Cu/graphene interface for high interaction strength. We expect that this study will enhance the understanding of the phonon-mediated thermal transport at metal/graphene interfaces and provide insights into tuning the TBC across MLG/metal interfaces.

### Acknowledgements

This work was partially supported by National Science Foundation Grant CBET-1236416.

### Notes and references

<sup>a</sup> G. W. Woodruff School of Mechanical Engineering, Georgia Institute of Technology, Atlanta, GA, United States.

<sup>b</sup> Dell Inc., Austin, TX, United States.

†Address correspondence to satish.kumar@me.gatech.edu

1. A. A. Balandin, *Nat Mater*, 2011, **10**, 569-581.
2. C. Lee, X. D. Wei, J. W. Kysar and J. Hone, *Science*, 2008, **321**, 385-388.
3. C. Yan, J. H. Cho and J. H. Ahn, *Nanoscale*, 2012, **4**, 4870-4882.
4. F. Bonaccorso, Z. Sun, T. Hasan and A. C. Ferrari, *Nature Photonics*, 2010, **4**, 611-622.
5. F. Schwierz, *Nat Nanotechnol*, 2010, **5**, 487-496.
6. J. X. Zheng, Y. Y. Wang, L. Wang, R. Quhe, Z. Y. Ni, W. N. Mei, Z. X. Gao, D. P. Yu, J. J. Shi and J. Lu, *Scientific Reports*, 2013, **3**, 2081.
7. Y. P. Liu, W. S. Lew and L. Sun, *Phys Chem Chem Phys*, 2011, **13**, 20208-20214.
8. A. Reina, X. T. Jia, J. Ho, D. Nezich, H. B. Son, V. Bulovic, M. S. Dresselhaus and J. Kong, *Nano Lett*, 2009, **9**, 30-35.
9. J. B. Hou, Y. Y. Shao, M. W. Ellis, R. B. Moore and B. L. Yi, *Phys Chem Chem Phys*, 2011, **13**, 15384-15402.
10. D. A. C. Brownson and C. E. Banks, *Phys Chem Chem Phys*, 2012, **14**, 8264-8281.
11. M. Freitag, M. Steiner, Y. Martin, V. Perebeinos, Z. H. Chen, J. C. Tsang and P. Avouris, *Nano Lett*, 2009, **9**, 1883-1888.
12. A. D. Liao, J. Z. Wu, X. R. Wang, K. Tahy, D. Jena, H. J. Dai and E. Pop, *Physical Review Letters*, 2011, **106**, 256801.
13. P. E. Hopkins, M. Baraket, E. V. Barnat, T. E. Beechem, S. P. Kearney, J. C. Duda, J. T. Robinson and S. G. Walton, *Nano Lett*, 2012, **12**, 590-595.
14. P. M. Norris, J. L. Smoyer, J. C. Duda and P. E. Hopkins, *Journal of Heat Transfer-Transactions of the Asme*, 2012, **134**, 020910.
15. A. J. Schmidt, K. C. Collins, A. J. Minnich and G. Chen, *J Appl Phys*, 2010, **107**, 104907.
16. J. J. Gengler, S. V. Shenogin, J. E. Bultman, A. K. Roy, A. A. Voevodin and C. Muratore, *J Appl Phys*, 2012, **112**, 094904.
17. L. Adamska, Y. Lin, A. J. Ross, M. Batzill and I. I. Oleynik, *Phys Rev B*, 2012, **85**, 195443.
18. R. Mao, B. D. Kong, C. Gong, S. Xu, T. Jayasekera, K. Cho and K. W. Kim, *Phys Rev B*, 2013, **87**, 165410.
19. M. Shen, P. K. Schelling and P. Keblinski, *Phys Rev B*, 2013, **88**, 045444.
20. Y. Chalopin, N. Mingo, J. K. Diao, D. Srivastava and S. Volz, *Appl Phys Lett*, 2012, **101**, 221903.
21. L. Chen, Z. Huang and S. Kumar, *Appl Phys Lett*, 2013, **103**, 123110.
22. G. Giovannetti, P. A. Khomyakov, G. Brocks, V. M. Karpan, J. van den Brink and P. J. Kelly, *Physical Review Letters*, 2008, **101**, 026803.
23. X. J. Liu, C. Z. Wang, M. Hupalo, W. C. Lu, M. C. Tringides, Y. X. Yao and K. M. Ho, *Phys Chem Chem Phys*, 2012, **14**, 9157-9166.
24. M. Harb, C. V. Schmising, H. Enquist, A. Jurgilaitis, I. Maximov, P. V. Shvets, A. N. Obraztsov, D. Khakhulin, M. Wulff and J. Larsson, *Appl Phys Lett*, 2012, **101**, 233108.
25. K. Sun, M. A. Stroschio and M. Dutta, *Superlattices and Microstructures*, 2009, **45**, 60-64.
26. G. Zhang and H. S. Zhang, *Nanoscale*, 2011, **3**, 4604-4607.
27. A. Allard and L. Wirtz, *Nano Lett*, 2010, **10**, 4335-4340.
28. L. Chen and S. Kumar, *J Appl Phys*, 2012, **112**, 043502.
29. J. Chen, G. Zhang and B. W. Li, *Nanoscale*, 2013, **5**, 532-536.
30. K. Chen, X. Wan, D. Q. Liu, Z. W. Kang, W. G. Xie, J. Chen, Q. Miao and J. B. Xu, *Nanoscale*, 2013, **5**, 5784-5793.
31. S. W. Chang, A. K. Nair and M. J. Buehler, *Journal of Physics-Condensed Matter*, 2012, **24**, 245301.
32. Y. X. Ni, Y. Chalopin and S. Volz, *Appl Phys Lett*, 2013, **103**, 141905.
33. Y. X. Ni, Y. Chalopin and S. Volz, *Appl Phys Lett*, 2013, **103**, 061906.
34. M. M. Sadeghi, M. T. Pettes and L. Shi, *Solid State Communications*, 2012, **152**, 1321-1330.
35. Z. Y. Wei, Z. H. Ni, K. D. Bi, M. H. Chen and Y. F. Chen, *Physics Letters A*, 2011, **375**, 1195-1199.
36. D. Singh, J. Y. Murthy and T. S. Fisher, *J Appl Phys*, 2011, **110**, 044317.
37. L. Lindsay, D. A. Broido and N. Mingo, *Phys Rev B*, 2011, **83**, 235428.
38. Y. K. Koh, M. H. Bae, D. G. Cahill and E. Pop, *Nano Lett*, 2010, **10**, 4363-4368.
39. M. Vanin, J. J. Mortensen, A. K. Kelkkanen, J. M. Garcia-Lastra, K. S. Thygesen and K. W. Jacobsen, *Phys Rev B*, 2010, **81**, 081408.
40. J. Lee, K. S. Novoselov and H. S. Shin, *Acs Nano*, 2011, **5**, 608-612.
41. Z. Huang, T. S. Fisher and J. Y. Murthy, *J Appl Phys*, 2010, **108**, 094319.
42. W. Zhang, T. S. Fisher and N. Mingo, *Numerical Heat Transfer Part B-Fundamentals*, 2007, **51**, 333-349.
43. W. Zhang, T. S. Fisher and N. Mingo, *Journal of Heat Transfer-Transactions of the Asme*, 2007, **129**, 483-491.
44. G. Kresse and J. Furthmuller, *Computational Materials Science*, 1996, **6**, 15-50.
45. T. F. Luo and G. Chen, *Phys Chem Chem Phys*, 2013, **15**, 3389-3412.
46. G. Kresse and D. Joubert, *Phys Rev B*, 1999, **59**, 1758-1775.
47. Z. P. Xu and M. J. Buehler, *Journal of Physics-Condensed Matter*, 2010, **22**, 485301.

48. W. A. Saidi, M. Lee, L. Li, G. W. Zhou and A. J. H. McGaughey, *Phys Rev B*, 2012, **86**, 245429.
49. H. J. Monkhorst and J. D. Pack, *Phys Rev B*, 1976, **13**, 5188-5192.
50. S. Plimpton, *Journal of Computational Physics*, 1995, **117**, 1-19.
51. L. Lindsay and D. A. Broido, *Phys Rev B*, 2010, **81**, 205441.
52. S. M. Foiles, M. I. Baskes and M. S. Daw, *Phys Rev B*, 1986, **33**, 7983-7991.
53. Z. P. Xu and M. J. Buehler, *Acs Nano*, 2009, **3**, 2767-2775.
54. Z. Y. Ong and E. Pop, *Phys Rev B*, 2010, **81**, 155408.
55. B. Silvi and A. Savin, *Nature*, 1994, **371**, 683-686.
56. A. Savin, R. Nesper, S. Wengert and T. F. Fassler, *Angewandte Chemie-International Edition in English*, 1997, **36**, 1809-1832.
57. S. N. Steinmann, Y. R. Mo and C. Corminboeuf, *Phys Chem Chem Phys*, 2011, **13**, 20584-20592.
58. Z. Huang, T. Fisher and J. Murthy, *J Appl Phys*, 2011, **109**, 074305.
59. R. Nicklow, H. G. Smith and Wakabaya.N, *Phys Rev B*, 1972, **5**, 4951-4962.
60. S. Shin, M. Kaviany, T. Desai and R. Bonner, *Phys Rev B*, 2010, **82**, 081302.